

One at A Time: Multi-step Volumetric Probability Distribution Diffusion for Depth Estimation

Bohan Li^{1,2} Jingxin Dong³ Yunnan Wang^{1,2} Jinming Liu^{1,2}
 Lianying Yin³ Wei Zhao³ Zheng Zhu⁴ Xin Jin² * Wenjun Zeng²
¹Shanghai Jiao Tong University ²Eastern Institute for Advanced Study
³Hunan University ⁴PhiGent Robotics

Abstract

Recent works have explored the fundamental role of depth estimation in multi-view stereo (MVS) and semantic scene completion (SSC). They generally construct 3D cost volumes to explore geometric correspondence in depth, and estimate such volumes in a single step relying directly on the ground truth approximation. However, such problem cannot be thoroughly handled in one step due to complex empirical distributions, especially in challenging regions like occlusions, reflections, etc. In this paper, we formulate the depth estimation task as a multi-step distribution approximation process, and introduce a new paradigm of modeling the **Volumetric Probability Distribution** progressively (step-by-step) following a Markov chain with **Diffusion models (VPDD)**. Specifically, to constrain the multi-step generation of volume in VPDD, we construct a meta volume guidance and a confidence-aware contextual guidance as conditional geometry priors to facilitate the distribution approximation. For the sampling process, we further investigate an online filtering strategy to maintain consistency in volume representations for stable training. Experiments demonstrate that our plug-and-play VPDD outperforms the state-of-the-arts for tasks of MVS and SSC, and can also be easily extended to different baselines to get improvement. It is worth mentioning that we are the first camera-based work that surpasses LiDAR-based methods on the SemanticKITTI dataset.

1 Introduction

Depth is among the most critical intermediate representations for 3D perception and broader computer vision tasks, such as multi-view stereo (MVS) [1, 2, 3] and semantic scene completion (SSC) [4, 5, 6]. To obtain accurate depth information, the current state-of-the-art methods tend to utilize 3D cost volumes to learn correspondence distribution across different depth hypothesis planes [7, 8]. Compared with these methods based on 2D contextual features [9, 10, 11], the 3D volumetric-based approaches efficiently leverage stereo geometric constraints through the matching process and achieve compelling results across different benchmark datasets [12, 13, 14]. Thus, how to achieve accurate 3D volumetric-based depth estimation is the focus of this work.

The existing volumetric-based works focused on using various sophisticated architecture [8, 2, 12] and loss functions [13, 15] to learn the volumetric correspondence distribution, which regards the estimation of 3D cost volumes as a single-step approximation process. However, simply forcing the estimated distribution to approximate the complex target distribution imposes a tremendous burden on the learning process, which cannot be thoroughly handled in one step for some complex challenging cases like occlusions, reflections, etc. On the other hand, generative diffusion models recently have exhibited a strong capability of probability distribution modeling in image generation based on a Markov chain [16, 17, 18, 19]. Specifically, the diffusion models construct intermediate target distribution at each step of the Markov chain, which subtly splits the learning of complex empirical

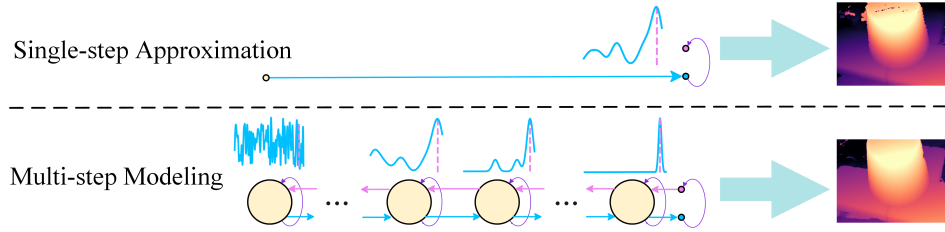


Figure 1: Comparison between single-step approximation and multi-step modeling (via diffusion). We demonstrate the estimated depth maps and the distribution approximation results of these two methods. We can see that multi-step modeling yields more accurate and reliable results.

distributions into multi-step distribution transition modeling [19, 20, 21]. This pipeline of multi-step modeling is exactly applicable to our volumetric distribution learning task, which could help us transform the complex cost volume prediction into progressive probabilistic distribution modeling.

Based on the above analysis, we propose a new concept of **Volumetric Probability Distribution Diffusion (VPDD)**, to achieve accurate depth estimation in MVS and SSC tasks. As shown in Figure 1, unlike the previous **single-step** approximation solutions, VPDD takes the volumetric distribution approximation as a **multi-step** generative process of conditional probabilistic distribution, which progressively constructs the correspondence of target cost volumes with the conditional constraints. Specifically, built upon the typical MVS [8, 22, 12, 13] or SSC [6] baselines, VPDD innovatively constructs the conditions with two kinds of guidance to lead the distribution transition, including a **Meta Volume Guidance (MVG)** and a **Confidence-aware Contextual Guidance (CCG)**. Particularly, MVG means we extract the coarse cost volumes from the pre-trained baselines as meta guidance (i.e., basic prior knowledge) and transform them into probabilistic form to condition the diffusion model for target distribution approximation. Despite the advance of MVG in high-confidence regions, the low-confidence mismatch issue in challenging regions (e.g. non-Lambertian surfaces, thin structures and reflections) still exists, which will impair the learning of probability distribution approximation to the target volumes. Therefore, CCG is further proposed to refine the predicted 3D volumes in VPDD with confidence-aware contexts. In detail, CCG first prunes the 3D volumes using confidence-aware filtering, and then, the fine-grained features and geometric details are retrieved from multi-scale contextual contents to supplement the information in the low-confidence regions of the volumes. Last, for the iterative sampling process in the diffusion of VPDD, we introduce an Online Filtering (OF) strategy to maintain the consistency of the inner representations for a stable diffusion to avoid perturbations during the progressive approximation to the ground truth volume. All in all, the main contributions of this paper are summarized as:

- We first pinpoint the issue of sing-step approximation of depth estimation, and correspondingly propose a new concept of Volumetric Probability Distribution Diffusion (VPDD), which progressively models complex depth volumes using multi-step generative diffusion to obtain a final accurate prediction.
- To construct the generative conditions for diffusion of VPDD, we further present a Meta Volume Guidance (MVG) and a Confidence-aware Contextual Guidance (CCG) as geometry priors to constrain the distribution approximation.
- For stable optimization, we design an Online Filtering (OF) strategy to maintain the representation consistency in the reverse sampling process of diffusion.

We evaluate our plug-and-play VPDD on two tasks of multi-view stereo (MVS) and semantic scene completion (SSC). Our method achieves state-of-the-art results on various benchmarks, including 1) MVS: DTU [23], BlendedMVS [24] and ScanNet [25]; 2) SSC: SemanticKITTI [26]. Besides, to the best of our knowledge, VPDD is the first camera-based method that surpasses LiDAR-based methods on the SemanticKITTI.

2 Related Works

2.1 Learning-based Depth Estimation

With the development of learning-based methods, the quality of depth estimation obtained from stereo matching has been steadily improved [27, 28, 29, 30, 31]. Broadly, stereo matching can be divided

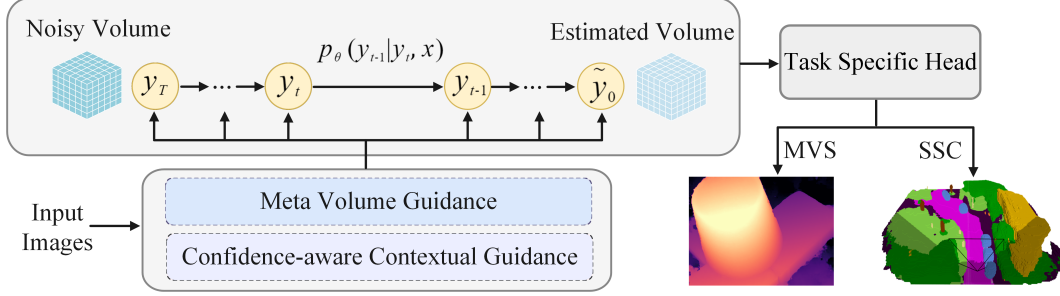


Figure 2: Overall framework of the proposed volumetric probability distribution diffusion (VPDD), where we progressively estimate an accurate volume over multiple steps via diffusing a noisy volume with conditional guidance. The estimated volumes are fed to the task-specific head to generate depth maps for multi-view stereo (MVS) or occupancy grids for semantic scene completion (SSC).

into binocular stereo and multi-view stereo depending on the number of input images [8, 32, 14]. Binocular stereo uses rectified stereo images as input and has recently been explored in semantic scene completion [4, 6, 5]. Voxformer [4] employs a two-stage framework where depth estimation is utilized to construct voxel queries in the first stage, and further guide dense voxels generation in the following stage. In the framework of StereoScene [6], a stereo volume constructor is proposed to generate a geometric cost volume to enhance the understanding of 3D scenarios.

In learning-based multi-view stereo, a set of images is employed to construct 3D cost volumes with epipolar constrain [1, 22, 8, 12, 13]. MVSNet [1] proposes to build variance-based cost volumes to measure similarity among multiple views. ESTD [22] constructs geometric correlations with temporal coherence using a epipolar spatio-temporal transformer for multi-view depth estimation. CasMVSNet [8] employs cascade cost volumes with different scales to form a coarse-to-fine depth estimation framework. TransMVSNet [12] leverages global context information with a feature matching transformer to exploit long-range aggregation across input images. To unify the volumetric distribution representation advantages of regression and classification, UniMVSNet [13] proposes a unification representation that is supervised with a unified focal loss. Different from previous methods that try to approximate the ground truth in a single step, we propose to formulate depth estimation as multi-step distribution modeling for performance improvement in challenging scenarios.

2.2 Denoising Diffusion Models

Denoising diffusion models (DDMs) are a novel class of deep generative models derived from nonequilibrium thermodynamics [33] and have achieved astounding results in the field of computer vision [16, 17, 18], natural language processing [34, 35, 36] and AI for science [37, 38]. DDMs model empirical data distribution by iterative denoising process [19] and closely resemble score-based generative models, which generate samples by Langevin dynamics based on estimated gradients of the data distribution [39]. Controlling the behavior of the vanilla diffusion models can optimize results on prediction tasks by designing additional conditions as guidance. For example, SR3 [20] produces photo-realistic samples on super-resolution tasks based on low-resolution images as the condition. DiffRF [21] adopts a set of posed images as additional conditions for radiance field synthesis with a rendering loss to resolve ambiguities. DiffuStereo [19] leverages an iterative diffusion model to obtain highly accurate depth maps for automatic high-quality human reconstruction from sparse-view inputs as conditions. However, DiffuStereo directly refines the depth maps generated by the off-the-shelf algorithms, without fully exploring the geometric constraints in the matching process. In contrast, we propose volumetric probability distribution diffusion (VPDD) to make full use of the correspondence distribution across different depth hypothesis planes.

3 Methodology

In this work, we formulate the depth estimation in MVS and SSC tasks as a multi-step conditional volumetric distribution learning. To this end, we introduce VPDD to learn a parametric approximation to the task-specific distribution progressively. As shown in Figure 2, VPDD predicts target volumes

taking noisy volumes with two conditions as guidance. The conditions are constructed from multi-view images based on MVS or SSC baselines, while the estimated volumes are fed to the task-specific head to generate depth maps in MVS or occupancy grids in SSC. Specifically, VPDD mainly consists of the following components to achieve compelling performance in volumetric-based depth estimation:

I. A Volumetric Diffusion model that learns the target volume approximation in a multi-step process, which is implemented with a 3D UNet [40, 21]. The volumetric diffusion model contains a forward process and a reverse sampling process. In the forward process, target volumes are constructed from ground truth depth maps. An **Online Filtering (OF)** strategy is further adopted to enhance performance in the reverse process.

II. A Meta Volume Guidance (MVG) and a **Confidence-aware Contextual Guidance (CCG)** as conditional guidance in VPDD. The meta volumes are constructed as basic geometry prior, while the confidence-aware context is further utilized to refine the estimated volumes in the 3D diffusion UNet.

3.1 Volumetric Diffusion

The standard generative diffusion models aim to form one-to-many mappings with a forward and reverse process. In our scenario, we employ a volumetric diffusion model to learn the parametric approximation to target volume based on the guidance of conditions.

In the forward process, we construct target unimodel volume \mathbf{y}_0 from ground truth depth map d^{gt} , and progressively corrupt the target volume to $\mathbf{y}_T \sim \mathcal{N}(\mathbf{0}, \mathbf{I})$ in T time steps. In the reverse process, the 3D diffusion UNet f_θ estimates $\tilde{\mathbf{y}}_0$ to approximate the target \mathbf{y}_0 from \mathbf{y}_T and we consider conditions \mathbf{x} to guide the estimation.

3.1.1 Volumetric Gaussian Forward Process

Given a ground truth depth map d^{gt} , we first construct the target volume \mathbf{y}_0 following the unimodel projection [12, 13] along depth dimension D as diffusion input:

$$\mathbf{y}_0 = Project^{Uni} \{d^{gt}, Dim = D\}, \quad (1)$$

We gradually add noise on \mathbf{y}_0 to generate the noisy volume \mathbf{y}_T over T steps following a discrete-time Markov chain. Given distribution of \mathbf{y}_0 , the forward process can be characterized as:

$$q(\mathbf{y}_t | \mathbf{y}_0) = \mathcal{N}(\mathbf{y}_t | \sqrt{\bar{\alpha}_t} \mathbf{y}_0, (1 - \bar{\alpha}_t) \mathbf{I}), \quad (2)$$

where $\bar{\alpha}_t = \prod_{i=1}^t \alpha_i$ and α_t is the pre-defined coefficient. \mathcal{N} and \mathbf{I} denote the normal distribution and the identical matrix, respectively.

3.1.2 Iterative Conditional Reverse Process

The conditional reverse sampling process is dedicated to iteratively denoise \mathbf{y}_T with conditions to recover \mathbf{y}_0 . Each step of the reverse process can be defined as conditional distribution transition [20], which is formulated as:

$$p_\theta(\mathbf{y}_{t-1} | \mathbf{y}_t, \mathbf{x}) = \mathcal{N}(\mathbf{y}_{t-1} | \mu_\theta(\mathbf{y}_t, \bar{\alpha}_t, \mathbf{x}), \sigma_t^2 \mathbf{I}), \quad (3)$$

where $\mu_\theta(\mathbf{y}_t, \bar{\alpha}_t, \mathbf{x}) = \frac{1}{\sqrt{\alpha_t}} \left(\mathbf{y}_t - \frac{1-\alpha_t}{\sqrt{1-\bar{\alpha}_t}} f_\theta(\mathbf{y}_t, \bar{\alpha}_t, \mathbf{x}) \right)$, and $\sigma^2 = \frac{(1-\bar{\alpha}_{t-1})(1-\alpha_t)}{1-\bar{\alpha}_t}$.

Online Filtering. Since VPDD is dedicated to learning for approximating the volume \mathbf{y}_0 with unimodel distribution, to suppress the perturbation on distribution transition by generated multi-model representation, we propose to filter the predicted \mathbf{y}_t online at each iteration before sending it to the next sampling step. Our implementation can be formally written as:

$$\mathbf{y}'_t = Project^{Uni} \{WTA^D(\mathbf{y}_t), Dim = D\}, \quad (4)$$

where $Project^{Uni}$ denotes unimodel projection same as GT volume construction in Section 3.1.1. WTA^D represents *Winner-Takes-All* operation [41], which maintains the unique peak along the depth dimension.

3.2 Conditional Guidance Construction

In this section, we introduce the condition construction in VPDD. We extract cost volumes and multi-scale contextual features from the off-the-shelf MVS or SSC baselines, and take them as conditions to constrain the learning of distribution transition in the diffusion process.

3.2.1 Meta Volume Guidance (MVG)

MVG aims to extract the basic prior knowledge to lead the diffusion model for a reasonable approximation in high-confidence regions. Given a cost volume \mathbf{V}_{cost} from baseline networks, we employ meta volume guidance to convert \mathbf{V}_{cost} into probabilistic form for the conditional diffusion process. The conversion is implemented with *softmax* along depth dimension for each pixel (h, w) in space, which is formally written as:

$$\mathbf{V}_{prob}^{h,w,m} = \text{Softmax}(\mathbf{V}_{cost}^{h,w,m}) = \frac{\exp(d_m^{h,w})}{\sum_{n=1}^{D_{max}} \exp(d_n^{h,w})}, \quad (5)$$

where $d_m^{h,w}$ represents cost value of m^{th} depth hypothesis plane ($1 < m < D_{max}$). D_{max} denotes the number of depth hypothesis planes. Please refer to Section 4.3 for more details about the selection of the probability conversion function. For multi-view stereo (MVS), we adopt regularized cost volumes [8, 22, 12, 13] as input, while the geometric cost volumes [6] are employed for semantic scene completion (SSC).

3.2.2 Confidence-aware Contextual Guidance (CCG)

Although the MVG constrains the distribution transition to some extent, it is still hard to achieve compelling results, especially in challenging regions like occlusions, reflections, textureless regions, etc. Thus, we propose confidence-aware contextual guidance to further apply continuous refinement on the estimated volumes in the reverse process.

The overall structure of confidence-aware contextual guidance is shown in Figure 3. Given a depth volume $\mathbf{V}_{depth}^i \in \mathbb{R}^{C \times D \times H \times W}$ in i^{th} downsample block of the 3D UNet (i.e., diffusion model) and i^{th} scale contextual features $\mathbf{F}_{context}^i \in \mathbb{R}^{C' \times H \times W}$ from feature extraction networks, our goal is to retrieval reliable contextual features from $\mathbf{F}_{context}^i$, and refine \mathbf{V}_{depth}^i according to confidence information along the spatial dimension. It is worth noting that we directly obtain multi-scale contextual features from the off-the-shelf baseline networks for computational efficiency.

Specifically, we first form a confidence map $\mathbf{C}^i \in \mathbb{R}^{C \times H \times W}$ by checking the highest probability value among all depth hypothesis planes across the depth dimension. Next, we reverse the values in \mathbf{C}^i to obtain query Q^i for cross attention that measures the matching uncertainty in \mathbf{V}_{depth}^i :

$$Q^i = \text{Sigmoid}(-\mathbf{C}^i) = \text{Sigmoid} \{ - (WTA^D(\mathbf{V}^i)) \}, \quad (6)$$

where WTA^D denotes *Winner-Takes-All* operation along depth dimension. To generate key K^i and value V^i , we apply deformable convolution on the corresponding contextual features $\mathbf{F}_{context}^i$ for efficient geometric transformation modeling and receptive fields adaption. For each location point \mathbf{p} on the contextual features $\mathbf{F}_{context}^i$, the process is formulated as:

$$K^i(\mathbf{p}), V^i(\mathbf{p}) = \text{Chunk} \left\{ \sum_{c=0}^{C'-1} W \cdot \mathbf{F}_{context}^i((\mathbf{p}) + \Delta(\mathbf{p}), \mathbf{c}), Dim = 1 \right\}, \quad (7)$$

where W and $\Delta(\mathbf{p})$ denotes the deformable weight and learnable offset, respectively. To reduce computation cost, we adopt linear attention [42, 43] as:

$$\mathbf{F}_{conf}^i = \text{LinearAtten}(Q^i, K^i, V^i) = \phi_q(Q^i) (\phi_k(K^i)^T V^i), \quad (8)$$

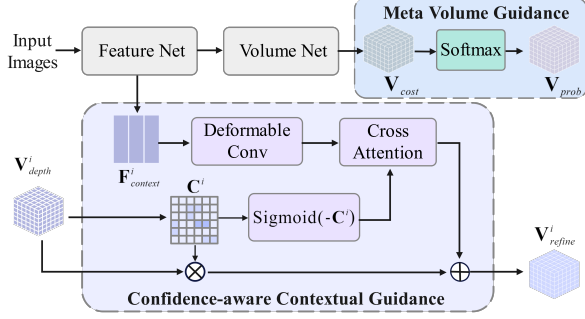


Figure 3: Illustration of the two kinds of conditional guidance construction in VPDD, which are both used to constrain the distribution transition in the diffusion process.

where \mathbf{F}_{conf}^i represents confidence-aware contextual features. ϕ_q and ϕ_k are *softmax* operations along each row and column of the input matrix, respectively. In this way, the relevant information of contextual features is retrieved according to the matching uncertainty of the depth volume \mathbf{V}_{depth}^i .

Subsequently, we implement multiplication between the depth volume \mathbf{V}_{depth}^i and confidence map \mathbf{C}^i to obtain a filtered volume. To match in dimension, \mathbf{F}_{conf}^i is projected into 3D contextual volume $\mathbf{V}_{context}^i$ before adding to the filtered volume following lift operation [44]. Finally, the refined volume is constructed by element-wise summation between the filtered volume and the contextual volume:

$$\mathbf{V}_{refine}^i = \mathbf{V}_{depth}^i \odot \mathbf{C}^i + \mathbf{V}_{context}^i, \quad (9)$$

where \odot denotes element-wise multiplication. Note that CCG is applied on each down-sample block of the 3D diffusion UNet with different dimension sizes. Through the refinement operation of CCG on the depth volume, volumetric distribution in high-confidence regions is retained, while that in low-confidence regions is optimized with multi-scale contexts.

3.3 Training Objective

In this work, we adopt an end-to-end joint training pipeline for the whole framework, and our training objective is to optimize the volumetric diffusion model for target volume approximation. Different loss functions are applied to achieve the object according to the representations of conditional meta volumes (in Section 3.2.1), which is consistent with baseline networks [8, 13, 12, 22, 6].

Regression Loss. For regression representation, we implement implicit supervision on the output of VPDD. Specifically, the estimated probabilistic depth volume is first regressed into a 2D depth map \tilde{d} , then a *SmoothL1* loss [8] is implemented between the estimated depth map \tilde{d} and the ground truth d^{gt} :

$$\mathcal{L}_{Regress} = \frac{1}{N} \sum_{i=1}^N \text{smooth}_{L1} \left(\tilde{d}_i - d_i^{gt} \right), \quad (10)$$

where N denotes the number of labeled pixels d_i^{gt} . In this way, the depth volume predicted by the volumetric diffusion model is implicitly supervised throughout the training process.

Classification Loss. For classification representation, we apply focal loss [12] to directly supervise discrete volumetric distribution. The function adopts a tunable parameter γ to help focus on hard samples to prevent overfitting, which is formally defined as:

$$\mathcal{L}_{Classify} = \sum_{\mathbf{p} \in \{\mathbf{p}_v\}} - \left(1 - P^{(\tilde{\mathbf{h}})}(\mathbf{p}) \right)^\gamma \log \left(P^{(\tilde{\mathbf{h}})}(\mathbf{p}) \right), \quad (11)$$

where \mathbf{p}_v and $\tilde{\mathbf{h}}$ denotes labeled pixels with valid ground truth and the depth hypothesis closest to the ground truth, respectively. $P^{(\tilde{\mathbf{h}})}(\mathbf{p})$ represents the prediction on depth hypothesis $\tilde{\mathbf{h}}$.

Unification Loss. For unification representation, we adopt unified focal loss [13] for continuous supervision on the estimated volume:

$$\mathcal{L}_{Unify} = \begin{cases} \alpha^+ (S_b^+ (\frac{|q-u|}{q^+}))^\gamma BCE(u, q), & q > 0 \\ \alpha^- (S_b^- (\frac{u}{q^+}))^\gamma BCE(u, q), & else \end{cases}. \quad (12)$$

where u and q denote estimated unity value and the continuous target, respectively. α and γ are tunable parameters for sample balance. BCE represents binary cross-entropy. $S_b(x)$ is a sigmoid-like function as $(1/(1 + b^{-x}))$.

4 Experiments

We evaluate the proposed *Volumetric Probability Distribution Diffusion (VPDD)* on the tasks of multi-view stereo (MVS) and semantic scene completion (SSC).

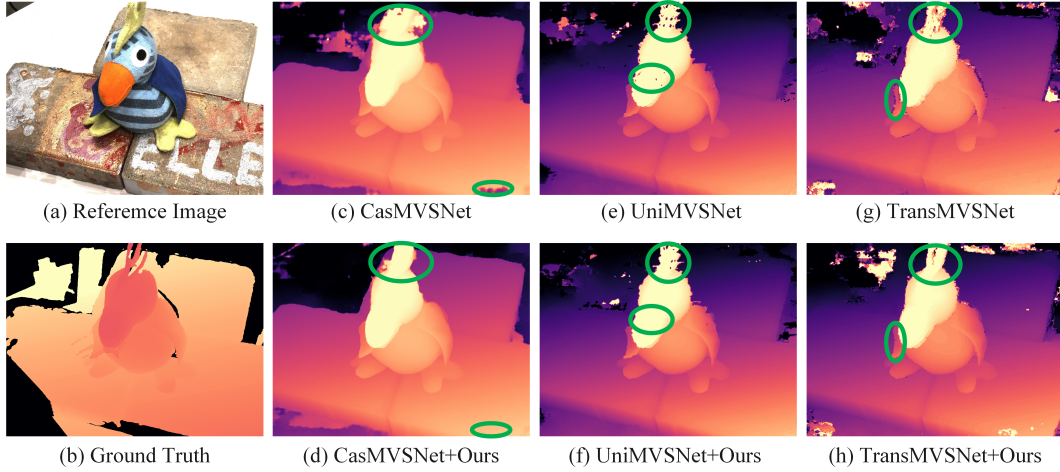


Figure 4: Qualitative results for MVS on the DTU test set. Different baseline networks are employed to evaluate the effectiveness of our proposed method. We can see that our proposed VPDD improves the quality of the estimated results on object boundaries and low-texture regions.

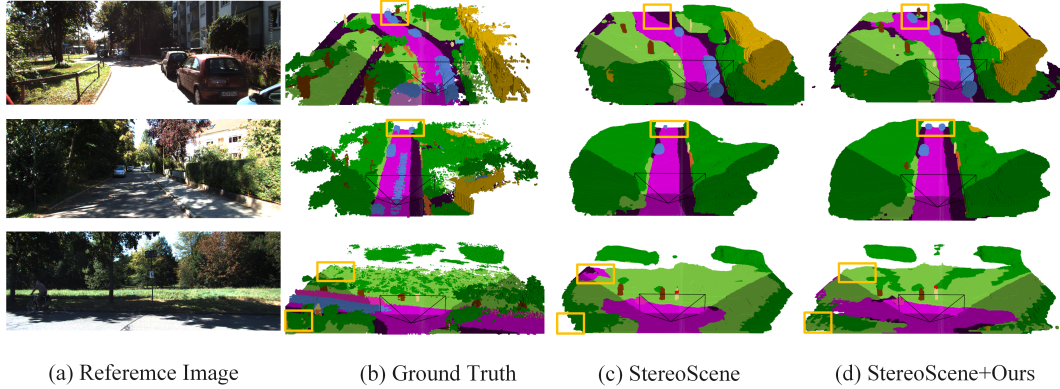


Figure 5: Qualitative results for SSC on the SemanticKITTI validation set. The shadow areas denote unseen scenery out of the camera’s field of view. Our proposed VPDD improves the performance of the baseline in challenging regions (e.g. textureless areas and small objects).

4.1 Multi-view Stereo

Datasets. DTU [23] is a large-scale indoor dataset, which consists of 124 different scenes with 7 different illumination conditions. We split the dataset into training, validation, and test set following the setting of MVSNet [1]. **BlendedMVS** [24] dataset is a synthetic dataset that consists of 106 training scans and 7 validation scans. **ScanNet** [25] is an RGB-D video dataset that consists of more than 1600 scans, annotated with depth maps and camera poses.

Implementation Details. Our model is implemented on the Pytorch platform with 4 NVIDIA A100 GPUs. We train our model for 16 epochs on DTU dataset and 7 epochs on the ScanNet dataset, respectively. For the BlendedMVS dataset, we implement tests using the model trained on the DTU dataset to evaluate the generalization ability. The initial learning rate is set to 2.5×10^{-5} , which decays following the same strategy of baseline networks. During the training process, the batch size is set to 12 and we adopt Adam as the optimizer. The diffusion forward step T is set to 1000 and we adopt 4 iterations in the reverse process.

Performance. For quantitative evaluation, we conduct standard metrics [45, 22, 46], including absolute relative error (Abs Rel), absolute error (Abs), square relative error (Sq Rel), root mean square error in linear scale (RMSE), threshold distance error (Th) and inlier ratios ($\delta < 1.25^i$, where $i \in \{1, 2\}$).

Quantitative results on the DTU test set are reported in Table 1. Our method shows significant improvements on baseline networks with different volume representations, including *regression distribution* of CasMVSNet [8, 22], *unified distribution* of UniMVSNet [13] and *classification distribution* of TransMVSNet [12]. Specifically, our method reduces Abs by 23.00%, 28.00%, and

31.46% on CasMVSNet, UniMVSNet, and TransMVSNet, respectively. Moreover, qualitative results in Figure 4 demonstrate our method improves the overall quality of the estimated depth maps, especially in challenging regions (e.g. object boundaries and low-texture areas).

We evaluate the zero-shot generalization ability of our method from DTU to BlendedMVS validation set without any fine-tuning. As shown in Table 2, our method has a notable performance gain compared to baseline networks, which demonstrates that our approach generalizes well across data without post-processing. Table 3 shows quantitative results on ScanNet test set. ESTD [22] with VPDD outperforms other methods in terms of accuracy, which indicates that our method also has strong modeling capability for temporal cost volumes.

Table 1: Quantitative results on the DTU test set for MVS. The best performers are marked **bold**.

Method	Abs Rel ↓	Abs ↓	Sq Rel ↓	Th8 ↓	Th20 ↓	$\delta_1 < 1.25 \uparrow$	$\delta_2 < 1.25^2 \uparrow$
MVSNet [1]	0.0139	11.5502	2.0383	0.1378	0.0932	0.9845	0.9966
CasMVSNet [8]	0.0097	7.4381	1.6300	0.0872	0.0570	0.9887	0.9976
UniMVSNet [13]	0.0095	7.2756	1.3163	0.0837	0.0547	0.9858	0.9934
TransMVSNet [12]	0.0094	7.2096	1.2712	0.0842	0.0541	0.9905	0.9982
CasMVSNet [8]+Ours	0.0075	5.7275	1.2439	0.0644	0.0414	0.9913	0.9981
UniMVSNet [13]+Ours	0.0071	5.2383	1.0402	0.0574	0.0404	0.9870	0.9940
TransMVSNet [12]+Ours	0.0067	4.9416	0.9918	0.0510	0.0333	0.9918	0.9984

Table 2: Zero-shot generalization from DTU to BlendedMVS for MVS.

Method	Abs Rel ↓	Abs ↓	$\delta_1 < 1.25 \uparrow$
MVSNet [1]	0.0915	2.6554	0.9135
CasMVSNet [8]	0.0665	1.7102	0.9349
UniMVSNet [13]	0.0825	1.8744	0.9320
TransMVSNet [12]	0.0657	1.9216	0.9402
CasMVSNet [8]+Ours	0.0404	1.4122	0.9604
UniMVSNet [13]+Ours	0.0496	1.3128	0.9425
TransMVSNet [12]+Ours	0.0376	1.2267	0.9596

Table 3: Quantitative results on the ScanNet test set for MVS.

Methods	Abs Rel ↓	Abs ↓	Sq Rel ↓	RMSE ↓	$\delta_1 < 1.25 \uparrow$
MVDepth [47]	0.1167	0.2301	0.0596	0.3236	0.8453
DPSNet [48]	0.1200	0.2104	0.0688	0.3139	0.8640
DELTA [49]	0.0915	0.1710	0.0327	0.2390	0.9147
NRGBD [50]	0.1013	0.1657	0.0502	0.2500	0.9160
PairNet [51]	0.0895	0.1709	0.0615	0.2734	0.9172
ESTD [22]	0.0812	0.1505	0.0298	0.2199	0.9313
ESTD [22]+Ours	0.0753	0.1497	0.0237	0.2149	0.9483

4.2 Semantic Scene Completion

Datasets. SemanticKITTI [26] is a popular semantic scene completion dataset, which contains 22 outdoor driving scenes. SemanticKITTI holds LiDAR annotations that are voxelized as $256 \times 256 \times 32$ grid of 0.2m voxels. The target voxel grids are labeled with 21 classes (1 free, 1 unknown, and 19 semantics). Following [6], we only adopt RGB images of the dataset as inputs.

Implementation Details. We extend StereoScene [6] with our proposed VPDD for SSC evaluation. More specifically, the geometric cost volume in StereoScene is leveraged for meta volume guidance construction. The whole model is trained on SemanticKITTI for 30 epochs with a learning rate of 2.5×10^{-5} . AdamW is adopted as a training optimizer following [6].

Table 4: Quantitative results on the SemanticKITTI validation set against the state-of-the-art SSC methods (higher is better). Our method even surpasses **LiDAR-based** SSCNet [52] with only camera-based inputs.

Method	road (15.30%)	sidewalk (11.13%)	parking (1.12%)	other-gnd (0.56%)	building (14.1%)	car (3.92%)	truck (0.16%)	bicycle (0.03%)	motorcycle (0.03%)	other-veh. (0.20%)	vegetation (39.3%)	trunk (0.51%)	terrain (9.17%)	person (0.07%)	bicyclist (0.07%)	motorcyclist. (0.05%)	fence (3.90%)	pole (0.29%)	traf.-sign (0.08%)	mIoU
MonoScene [53]	55.89	26.50	14.75	1.63	13.55	23.29	9.29	0.28	0.59	2.63	17.98	2.44	29.84	2.00	1.07	0.00	6.60	3.91	2.43	11.30
VoxFormer-T [4]	53.57	26.52	19.69	0.42	19.54	26.54	7.26	1.28	0.56	7.81	26.10	6.10	33.06	1.93	1.97	0.00	7.31	9.15	4.94	13.35
SSCNet [52]	-	-	-	-	-	-	-	-	-	-	-	-	-	-	-	-	-	-	-	16.35
StereoScene [6]	58.31	28.20	21.48	0.09	21.62	26.32	19.77	3.04	3.77	9.25	23.52	7.18	35.90	5.20	2.70	0.00	10.87	9.72	6.32	15.43
StereoScene [6]+Ours	62.30	30.97	21.96	0.59	23.92	30.86	18.96	2.53	3.29	12.24	25.35	7.96	36.23	2.80	3.39	0.00	10.14	10.95	6.51	16.37

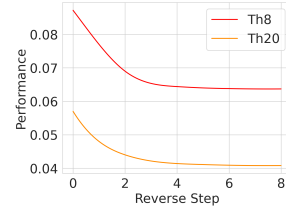
Performance. For quantitative evaluation, we adopt mIoU (mean Intersection over Union) to account for the SSC task. We compare our method with other state-of-the-art SSC networks: (1) camera-based methods including MonoScene [53], VoxFormer-T [4] and StereoScene [6], (2) LiDAR-based method

of SSCNet [52]. As shown in Table 4, our method surpasses StereoScene by 6.09% in terms of mIoU, which demonstrates the application of VPDD effectively improves the accuracy of depth estimation and thereby enhances the performance of semantic scene completion. It’s worth noting that our method even surpasses the LiDAR-based method of SSCNet in terms of mIoU. Figure 5 visualizes the qualitative results, our method produces more accurate and complete results in large-scale driving scenarios compared with StereoScene.

Table 5: Ablation study for different model settings.

Model Settings					Evaluation Metrics	
$MVG_{Sigmoid}$	MVG_{Norm}	$MVG_{Softmax}$	CCG	OF	Abs Rel ↓	Abs ↓
✓					0.0124	9.7147
	✓				0.0098	7.5126
		✓			0.0105	8.5242
		✓			0.0083	6.3111
		✓	✓		0.0078	5.9829
		✓	✓	✓	0.0075	5.7275

Figure 6: Ablation results for different reverse steps.



4.3 Ablation Study

We conduct extensive ablation studies on DTU test set with different model settings. We extend CasMVSNet with VPDD of different settings for the evaluation.

Effect of Architecture Settings. For the setting in the first row, we adopt cost volume without probabilistic conversion as the only additional condition. The reverse iterations are set to 4 unless otherwise stated. As shown in Table 5, it is necessary to convert conditional cost volume into probabilistic form as meta volume guidance, while the absence of probabilistic conversion causes a significant performance drop. The CCG and OF also obviously enhance the depth estimation performance, reducing Abs by 5.20% and 4.27%, respectively.

Effect of Meta Volume Conversion Strategy. Due to the mutual exclusivity of the distributions in different depth hypothesis planes, *softmax* is appropriate for meta volume conversion in depth estimation. In principle, other strategies can also accomplish the conversion for VPDD. We present *Sigmoid* and *Normalization* as alternative options: I. $\mathbf{V}_{prob}^{h,w,m} = Sigmoid(\mathbf{V}_{cost}^{h,w,m}) = 1/(1 + \exp(-d_m^{h,w}))$, II. $\mathbf{V}_{prob}^{h,w,m} = Norm(\mathbf{V}_{cost}^{h,w,m}) = d_m^{h,w}/(MAX(\mathbf{V}_{cost}^{h,w}))$.

As shown in Table 5, *Softmax* is the most efficient strategy for the conversion in depth estimation as speculated. The other two conversion strategies may facilitate VPDD to be more applicable in other tasks, which we leave to future work.

Effect of Reverse Steps. We also ablate our model with different reverse steps. As shown in Figure 6, our model is very efficient in the reverse process and achieves compelling results in a few steps. The relative performance gain from the reverse iteration gradually decreases around 4 steps, thus we adopt 4 iterations when comparing with other methods to balance between efficiency and effectiveness.

5 Conclusion

In this work, we propose a plug-and-play method of volumetric probability distribution diffusion (VPDD) for depth estimation in multi-view stereo (MVS) and semantic scene completion (SSC). Different from previous single-step approximation solutions, we employ multi-step generative diffusion to progressively model volumetric probability distribution for more accurate depth prediction. Technically, we construct a meta volume guidance (MVG) and a confidence-awareness contextual guidance (CCG) to condition the volumetric diffusion model for a reasonable target volume approximation. In the sampling process, we further propose an online filtering (OF) strategy to maintain consistency in estimated volume representations. Our method achieves state-of-the-art performance on multiple MVS/SSC benchmarks and even surpasses LiDAR-based method with only camera-based inputs.

References

- [1] Yao Yao, Zixin Luo, Shiwei Li, Tian Fang, and Long Quan. Mvsnet: Depth inference for unstructured multi-view stereo. In *ECCV*, 2018. 1, 3, 7, 8
- [2] Po-Heng Chen, Hsiao-Chien Yang, Kuan-Wen Chen, and Yong-Sheng Chen. Mvsnet++: Learning depth-based attention pyramid features for multi-view stereo. *IEEE Transactions on Image Processing*, 29, 2020. 1
- [3] Youmin Zhang, Yimin Chen, Xiao Bai, Suihanjin Yu, Kun Yu, Zhiwei Li, and Kuiyuan Yang. Adaptive unimodal cost volume filtering for deep stereo matching. In *AAAI*, 2020. 1
- [4] Yiming Li, Zhiding Yu, Christopher Choy, Chaowei Xiao, Jose M Alvarez, Sanja Fidler, Chen Feng, and Anima Anandkumar. Voxformer: Sparse voxel transformer for camera-based 3d semantic scene completion. *CVPR*, 2023. 1, 3, 8
- [5] Ruihang Miao, Weizhou Liu, Mingrui Chen, Zheng Gong, Weixin Xu, Chen Hu, and Shuchang Zhou. Occdepth: A depth-aware method for 3d semantic scene completion. *arXiv preprint arXiv:2302.13540*, 2023. 1, 3
- [6] Bohan Li, Yasheng Sun, Xin Jin, Wenjun Zeng, Zheng Zhu, Xiaofeng Wang, Yunpeng Zhang, James Okae, Hang Xiao, and Dalong Du. Stereoscene: Bev-assisted stereo matching empowers 3d semantic scene completion. *arXiv preprint arXiv:2303.13959*, 2023. 1, 2, 3, 5, 6, 8
- [7] Zhichao Yin, Trevor Darrell, and Fisher Yu. Hierarchical discrete distribution decomposition for match density estimation. In *CVPR*, pages 6044–6053, 2019. 1
- [8] Xiaodong Gu, Zhiwen Fan, Siyu Zhu, Zuozhuo Dai, Feitong Tan, and Ping Tan. Cascade cost volume for high-resolution multi-view stereo and stereo matching. In *CVPR*, 2020. 1, 2, 3, 5, 6, 7, 8
- [9] Nikolaus Mayer, Eddy Ilg, Philip Hausser, Philipp Fischer, Daniel Cremers, Alexey Dosovitskiy, and Thomas Brox. A large dataset to train convolutional networks for disparity, optical flow, and scene flow estimation. In *CVPR*, 2016. 1
- [10] Qiang Wang, Shaohuai Shi, Shizhen Zheng, Kaiyong Zhao, and Xiaowen Chu. Fadnet: A fast and accurate network for disparity estimation. In *ICRA*, 2020. 1
- [11] Fangjinhua Wang, Silvano Galliani, Christoph Vogel, Pablo Speciale, and Marc Pollefeys. Patchmatchnet: Learned multi-view patchmatch stereo. In *CVPR*, 2021. 1
- [12] Yikang Ding, Wentao Yuan, Qingtian Zhu, Haotian Zhang, Xiangyue Liu, Yuanjiang Wang, and Xiao Liu. Transmvsnet: Global context-aware multi-view stereo network with transformers. In *CVPR*, 2022. 1, 2, 3, 4, 5, 6, 7, 8
- [13] Rui Peng, Rongjie Wang, Zhenyu Wang, Yawen Lai, and Ronggang Wang. Rethinking depth estimation for multi-view stereo: A unified representation. In *CVPR*, 2022. 1, 2, 3, 4, 5, 6, 7, 8
- [14] Gangwei Xu, Xianqi Wang, Xiaohuan Ding, and Xin Yang. Iterative geometry encoding volume for stereo matching. In *CVPR*, 2023. 1, 3
- [15] Xiaofeng Wang, Zheng Zhu, Guan Huang, Fangbo Qin, Yun Ye, Yijia He, Xu Chi, and Xingang Wang. Mvster: epipolar transformer for efficient multi-view stereo. In *ECCV*, 2022. 1
- [16] Shitong Luo and Wei Hu. Diffusion probabilistic models for 3d point cloud generation. In *CVPR*, pages 2837–2845, 2021. 1, 3
- [17] Robin Rombach, Andreas Blattmann, Dominik Lorenz, Patrick Esser, and Björn Ommer. High-resolution image synthesis with latent diffusion models. In *CVPR*, pages 10684–10695, 2022. 1, 3
- [18] Aditya Ramesh, Mikhail Pavlov, Gabriel Goh, Scott Gray, Chelsea Voss, Alec Radford, Mark Chen, and Ilya Sutskever. Zero-shot text-to-image generation. In *International Conference on Machine Learning*, pages 8821–8831. PMLR, 2021. 1, 3

- [19] Ruizhi Shao, Zerong Zheng, Hongwen Zhang, Jingxiang Sun, and Yebin Liu. Diffustereo: High quality human reconstruction via diffusion-based stereo using sparse cameras. In *ECCV 2022*, 2022. 1, 2, 3
- [20] Chitwan Saharia, Jonathan Ho, William Chan, Tim Salimans, David J Fleet, and Mohammad Norouzi. Image super-resolution via iterative refinement. *IEEE Transactions on Pattern Analysis and Machine Intelligence*, 2022. 2, 3, 4
- [21] Norman Müller, Yawar Siddiqui, Lorenzo Porzi, Samuel Rota Bulò, Peter Kotschieder, and Matthias Nießner. Diffrrf: Rendering-guided 3d radiance field diffusion. 2023. 2, 3, 4
- [22] Xiaoxiao Long, Lingjie Liu, Wei Li, Christian Theobalt, and Wenping Wang. Multi-view depth estimation using epipolar spatio-temporal networks. In *CVPR*, pages 8258–8267, 2021. 2, 3, 5, 6, 7, 8
- [23] Henrik Aanæs, Rasmus Jensen, George Vogiatzis, Engin Tola, and Anders Dahl. Large-scale data for multiple-view stereopsis. *International Journal of Computer Vision*, 2016. 2, 7
- [24] Yao Yao, Zixin Luo, Shiwei Li, Jingyang Zhang, Yufan Ren, Lei Zhou, Tian Fang, and Long Quan. Blendedmvs: A large-scale dataset for generalized multi-view stereo networks. In *CVPR*, 2020. 2, 7
- [25] Angela Dai, Angel X Chang, Manolis Savva, Maciej Halber, Thomas Funkhouser, and Matthias Nießner. Scannet: Richly-annotated 3d reconstructions of indoor scenes. In *CVPR*, 2017. 2, 7
- [26] Jens Behley, Martin Garbade, Andres Milioto, Jan Quenzel, Sven Behnke, Cyrill Stachniss, and Jurgen Gall. Semantickitti: A dataset for semantic scene understanding of lidar sequences. In *ICCV*, 2019. 2, 8
- [27] Jure Zbontar and Yann LeCun. Computing the stereo matching cost with a convolutional neural network. In *CVPR*, 2015. 2
- [28] Nikolaus Mayer, Eddy Ilg, Philip Häusser, Philipp Fischer, Daniel Cremers, Alexey Dosovitskiy, and Thomas Brox. A large dataset to train convolutional networks for disparity, optical flow, and scene flow estimation. *CVPR*, 2016. 2
- [29] Hongwei Yi, Zizhuang Wei, Mingyu Ding, Runze Zhang, Yisong Chen, Guoping Wang, and Yu-Wing Tai. Pyramid multi-view stereo net with self-adaptive view aggregation. In *ECCV*, 2020. 2
- [30] Lahav Lipson; Zachary Teed; Jia Deng. Raft-stereo: Multilevel recurrent field transforms for stereo matching. *3DV*, 2021. 2
- [31] Jiankun Li, Peisen Wang, Pengfei Xiong, Tao Cai, Ziwei Yan, Lei Yang, Jiangyu Liu, Haoqiang Fan, and Shuaicheng Liu. Practical stereo matching via cascaded recurrent network with adaptive correlation. *CVPR*, 2021. 2
- [32] Matteo Poggi, Fabio Tosi, Konstantinos Batsos, Philippos Mordohai, and Stefano Mattoccia. On the synergies between machine learning and binocular stereo for depth estimation from images: A survey. *IEEE Transactions on Pattern Analysis and Machine Intelligence*, 2022. 3
- [33] Jascha Sohl-Dickstein, Eric Weiss, Niru Maheswaranathan, and Surya Ganguli. Deep unsupervised learning using nonequilibrium thermodynamics. In *ICML*. PMLR, 2015. 3
- [34] Xiang Li, John Thickstun, Ishaan Gulrajani, Percy S Liang, and Tatsunori B Hashimoto. Diffusion-lm improves controllable text generation. *NeurIPS*, 35:4328–4343, 2022. 3
- [35] Shansan Gong, Mukai Li, Jiangtao Feng, Zhiyong Wu, and Lingpeng Kong. DiffuSeq: Sequence to sequence text generation with diffusion models. In *ICLR*, 2023. 3
- [36] Machel Reid, Vincent J Hellendoorn, and Graham Neubig. Diffuser: Discrete diffusion via edit-based reconstruction. *arXiv preprint arXiv:2210.16886*, 2022. 3
- [37] Shitong Luo, Chence Shi, Minkai Xu, and Jian Tang. Predicting molecular conformation via dynamic graph score matching. *NeurIPS*, 34:19784–19795, 2021. 3

- [38] Minkai Xu, Lantao Yu, Yang Song, Chence Shi, Stefano Ermon, and Jian Tang. Geodiff: A geometric diffusion model for molecular conformation generation. In *ICLR*, 2022. 3
- [39] Hao Jiang and Yadong Mu. Conditional diffusion process for inverse halftoning. *NeurIPS*, 35: 5498–5509, 2022. 3
- [40] Olaf Ronneberger, Philipp Fischer, and Thomas Brox. U-net: Convolutional networks for biomedical image segmentation. In *MICCAI*, 2015. 4
- [41] Xuelian Cheng, Yiran Zhong, Mehrtash Harandi, Yuchao Dai, Xiaojun Chang, Hongdong Li, Tom Drummond, and Zongyuan Ge. Hierarchical neural architecture search for deep stereo matching. *NeurIPS*, 33, 2020. 4
- [42] Nikita Kitaev, Lukasz Kaiser, and Anselm Levskaya. Reformer: The efficient transformer. In *ICLR*, 2020. 5
- [43] Zhuoran Shen, Mingyuan Zhang, Haiyu Zhao, Shuai Yi, and Hongsheng Li. Efficient attention: Attention with linear complexities. In *WACV*, 2021. 5
- [44] Jonah Philion and Sanja Fidler. Lift, splat, shoot: Encoding images from arbitrary camera rigs by implicitly unprojecting to 3d. In *ECCV*, 2020. 6
- [45] David Eigen, Christian Puhrsch, and Rob Fergus. Depth map prediction from a single image using a multi-scale deep network. *NeurIPS*, 27, 2014. 7
- [46] Changjiang Cai, Pan Ji, and Yi Xu. Riav-mvs: Recurrent-indexing an asymmetric volume for multi-view stereo. *CVPR*, 2023. 7
- [47] Kaixuan Wang and Shaojie Shen. Mvdepthnet: Real-time multiview depth estimation neural network. In *3DV*, 2018. 8
- [48] Sunghoon Im, Hae-Gon Jeon, Stephen Lin, and In So Kweon. Dpsnet: End-to-end deep plane sweep stereo. *arXiv preprint arXiv:1905.00538*, 2019. 8
- [49] Ayan Sinha, Zak Murez, James Bartolozzi, Vijay Badrinarayanan, and Andrew Rabinovich. Depth estimation by learning triangulation and densification of sparse points for multi-view stereo. *arXiv preprint arXiv:2003.08933*, 2020. 8
- [50] Chao Liu, Jinwei Gu, Kihwan Kim, Srinivasa G Narasimhan, and Jan Kautz. Neural rgb (r) d sensing: Depth and uncertainty from a video camera. In *CVPR*, 2019. 8
- [51] Fangjinhua Wang, Silvano Galliani, Christoph Vogel, and Marc Pollefeys. Itermvs: iterative probability estimation for efficient multi-view stereo. In *CVPR*, 2022. 8
- [52] Shuran Song, Fisher Yu, Andy Zeng, Angel X Chang, Manolis Savva, and Thomas Funkhouser. Semantic scene completion from a single depth image. In *CVPR*, 2017. 8, 9
- [53] Anh-Quan Cao and Raoul de Charette. Monoscene: Monocular 3d semantic scene completion. In *CVPR*, 2022. 8

Supplementary Material for Multi-step Volumetric Probability Distribution Diffusion

Anonymous Author(s)

Affiliation

Address

email

A Volumetric Diffusion Architectural Details

We adopt a 3D UNet [?] as the architecture of the volumetric diffusion model in Section 3.1 of the main paper. As shown in Figure 1, the 3D UNet consists of three downsample and upsample blocks. Each downsample block contains two residual layers [?] and a CCG layer for the contextual guidance, while each upsample block contains two residual layers. The CCG takes contextual features $\mathbf{F}_{context}^i$ as inputs to refine the estimated depth volumes in the 3D UNet. The downsample blocks adopt 3D convolutions with stride two for downsampling, and the upsample blocks use trilinear interpolation for upsampling. We employ Group Norm [?] and SiLU [?] in each block for normalization and activation, respectively. Moreover, MVG generates the conditional probabilistic volume from the given cost volume \mathbf{V}_{cost} , which is concatenated with the input noisy volume \mathbf{y}_t before feeding into the 3D UNet.

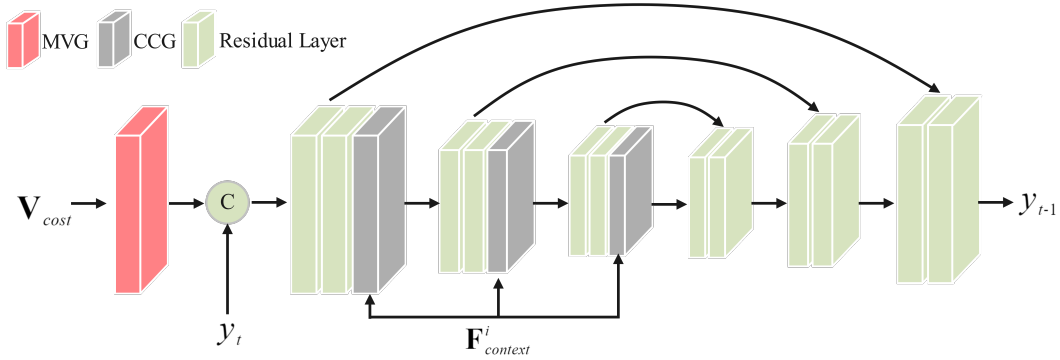


Figure 1: Architectural details of the 3D diffusion UNet.

B Additional Visualization Results on CCG

As described in Section 3.2.2 of the main paper, we employ CCG to continuously refine the estimated volumes. We conduct additional experiments to demonstrate the effect of CCG based on CasMVSNet [?]. In Figure 2, we show the confidence map \mathbf{C}^i , uncertainty map $\text{Sigmoid}(-\mathbf{C}^i)$, estimated depth map without CCG and estimated depth map with CCG. It can be seen that the model without CCG struggles to achieve compelling results in challenging regions (e.g. object boundaries, low-texture regions). The confidence map and the uncertainty map illustrate the regions with poor estimation, which are effectively refined by retrieving information from the contextual features with CCG.

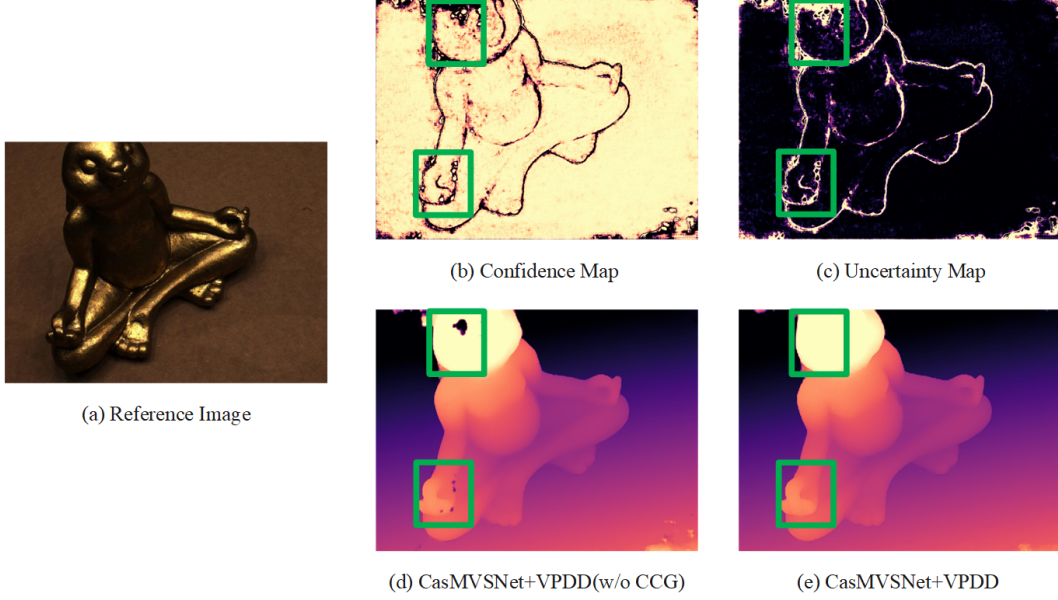


Figure 2: Visualization results of CCG.

20 C Additional Qualitative Results

21 We provide additional qualitative results for MVS and SSC. The results further demonstrate the
 22 effectiveness of our approach in enhancing the depth estimation performance.

23 **Multi-view Stereo.** We visualize more qualitative results on DTU [?] test set in Figure 3 and
 24 BlendedMVS [?] validation set in Figure 4. For the tests on BlendedMVS dataset, we use the model
 25 trained on DTU dataset to evaluate the generalization ability. Compared with the baseline networks,
 26 our method generates more complete depth maps and achieves more accurate results in challenging
 27 regions (e.g., object boundaries, repetitive pattern regions).

28 **Semantic Scene Completion.** We visualize more qualitative results on SemanticKITTI validation
 29 set in Figure 5. Compared to StereoScene [?], our method shows obvious advancement on small
 30 moving objects (e.g., trucks in row 2, cars in row 1 and row 5) and generates more accurate 3D scene
 31 layout (e.g., roads in row 3 and row 4).

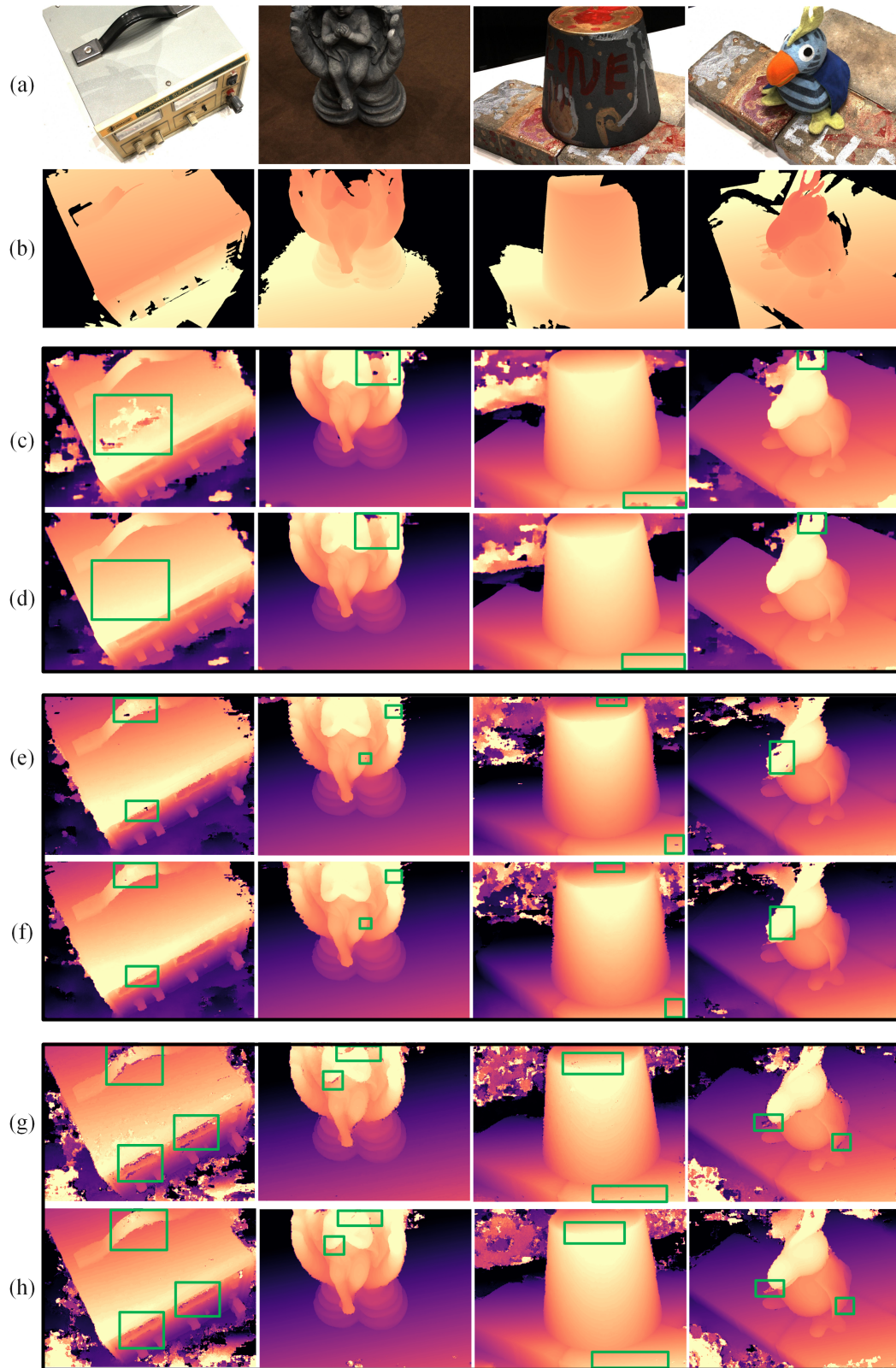


Figure 3: More visualization results on the DTU [?] test set. From top to bottom, (a) reference images, (b) ground truth, (c) CasMVSNet [?] results, (d) CasMVSNet [?] + VPDD results, (e) UniMVSNet [?] results, (f) UniMVSNet [?] + VPDD results, (g) TransMVSNet [?] results, (h) TransMVSNet [?] + VPDD results.

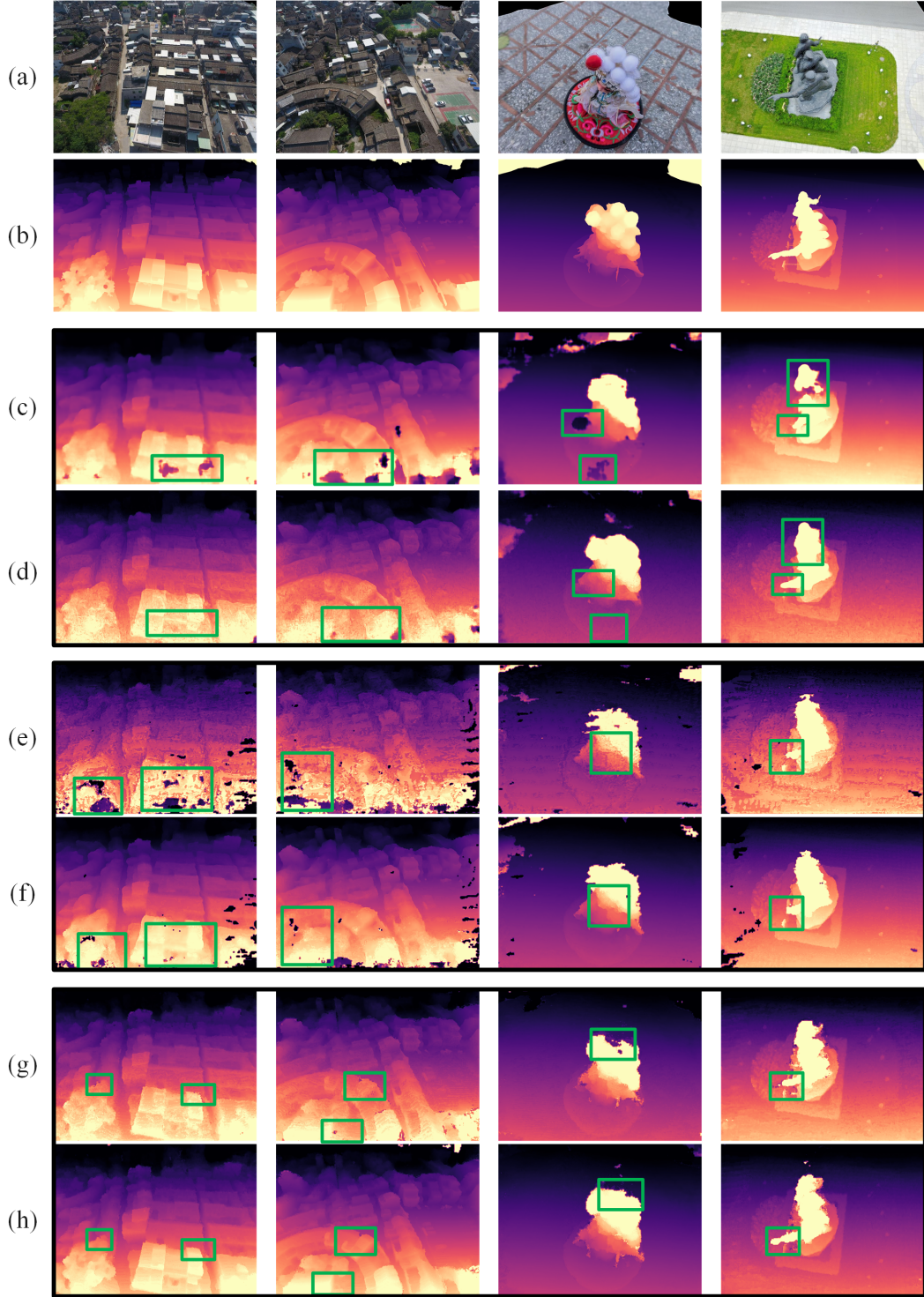


Figure 4: More visualization results on the BlendedMVS [?] validation set. From top to bottom, (a) reference images, (b) ground truth, (c) CasMVSNet [?] results, (d) CasMVSNet [?] + VPDD results, (e) UniMVSNet [?] results, (f) UniMVSNet [?] + VPDD results, (g) TransMVSNet [?] results, (h) TransMVSNet [?] + VPDD results.

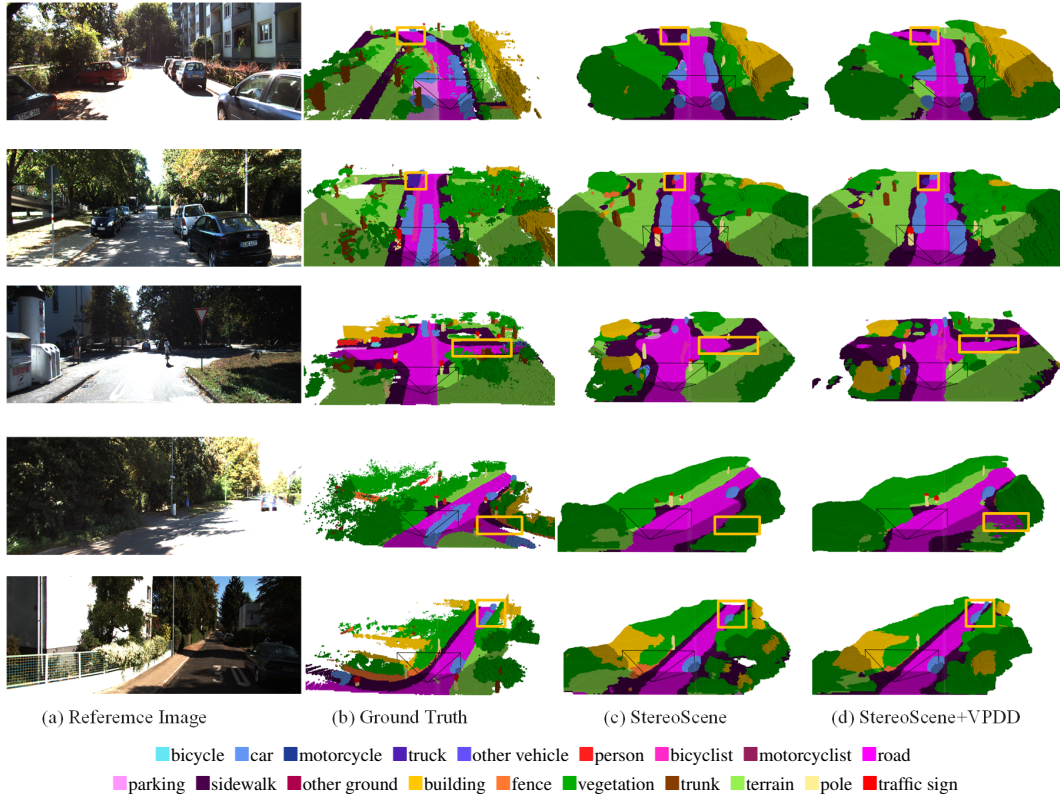


Figure 5: More visualization results on the SemanticKITTI [?] validation set. The shadow areas denote unseen scenery out of the camera’s field of view.